

# Regeneration Based Training-free Attribution of Fake Images Generated by Text-to-Image Generative Models

Meiling Li  
Fudan University  
Shanghai, China  
mlli20@fudan.edu.cn

Zhenxing Qian\*  
Fudan University  
Shanghai, China  
zxqian@fudan.edu.cn

Xinpeng Zhang†  
Fudan University  
Shanghai, China  
zhangxinpeng@fudan.edu.cn

## ABSTRACT

Text-to-image generative models have recently garnered significant attention due to their ability to generate images based on prompt descriptions. While these models have shown promising performance, concerns have been raised regarding the potential misuse of the generated fake images. In response to this, we have presented a simple yet effective training-free method to attribute fake images generated by text-to-image models to their source models. Given a test image to be attributed, we first inverse the textual prompt of the image, and then put the reconstructed prompt into different candidate models to regenerate candidate fake images. By calculating and ranking the similarity of the test image and the candidate images, we can determine the source of the image. This attribution allows model owners to be held accountable for any misuse of their models. Note that our approach does not limit the number of candidate text-to-image generative models. Comprehensive experiments reveal that (1) Our method can effectively attribute fake images to their source models, achieving comparable attribution performance with the state-of-the-art method; (2) Our method has high scalability ability, which is well adapted to real-world attribution scenarios. (3) The proposed method yields satisfactory robustness to common attacks, such as Gaussian blurring, JPEG compression, and Resizing. We also analyze the factors that influence the attribution performance, and explore the boost brought by the proposed method as a plug-in to improve the performance of existing SOTA. We hope our work can shed some light on the solutions to addressing the source of AI-generated images, as well as to prevent the misuse of text-to-image generative models. The code will be released after the paper is accepted.

\*Corresponding author.

†Corresponding author.

Permission to make digital or hard copies of all or part of this work for personal or classroom use is granted without fee provided that copies are not made or distributed for profit or commercial advantage and that copies bear this notice and the full citation on the first page. Copyrights for components of this work owned by others than the author(s) must be honored. Abstracting with credit is permitted. To copy otherwise, or republish, to post on servers or to redistribute to lists, requires prior specific permission and/or a fee. Request permissions from [permissions@acm.org](mailto:permissions@acm.org).

Conference'17, July 2017, Washington, DC, USA

© 2024 Copyright held by the owner/author(s). Publication rights licensed to ACM.

ACM ISBN 978-1-4503-XXXX-X/18/06...\$15.00

<https://doi.org/XXXXXXXX.XXXXXXX>

## CCS CONCEPTS

• Security and privacy → Social aspects of security and privacy.

## KEYWORDS

Text-to-Image Generative Models, Fake Image Attribution, AIGC

ACM Reference Format:

Meiling Li, Zhenxing Qian, and Xinpeng Zhang. 2024. Regeneration Based Training-free Attribution of Fake Images Generated by Text-to-Image Generative Models. In Proceedings of ACM Conference (Conference'17). ACM, New York, NY, USA, 14 pages. <https://doi.org/XXXXXXXX.XXXXXXX>

## 1 INTRODUCTION

Text-to-image generation models, such as Stable Diffusion [20], GLIDE [15], and DALL·E 2 [18], have advanced significantly, producing high-quality images from textual prompts. While traditional Generative Adversarial Networks (GANs) generate synthetic images from a Gaussian distribution, text-to-image models require textual prompts to create matching images and, hence they are used more widely with higher popularity. These synthetic images have diverse applications, including visualizing novel scenes, generating illustrations for advertising, and creating unphotographable scenes. However, these synthetic images also present societal risks, as they can be misused for spreading misinformation. Also, text-to-image generative models may impact the art industry by producing fake artwork. Therefore, we need to know by which model the AI-generated image is generated (Figure 1). That is, we need to attribute the unknown-source image to its source model correctly.

Through post-hoc analysis of differences in the intrinsic characteristics of the content generated by different generative models, we can determine the source of the generated content. So far, the research tailored for attributing AI-generated images is mostly training-based, which mainly focuses on the ownership of images generated by Generative Adversarial Network (GAN) models. Some studies use classification networks to determine the source of generated content based on the inherent feature differences of images generated by different models. Yu et al. [31] designed three variant classification networks based on mainstream convolutional neural networks, capable of attributing images generated by four common GAN models. Girish et al. [7] proposed an iterative framework for discovering images generated by unknown GANs, incorporating trainable networks, outlier detection,

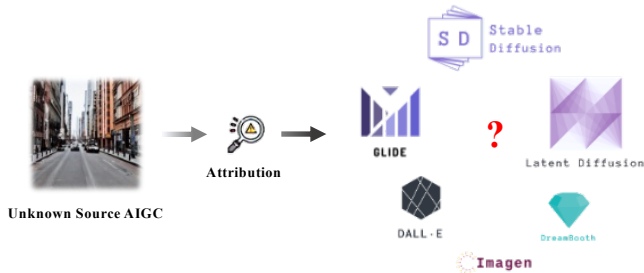


Figure 1: The application scenario of the AI-generated fake image attribution.

clustering, merging, and optimization modules. Bui et al. [2] introduced a GAN fingerprint technology called RepMix based on representation blending and a novel loss function, which significantly improves semantic generalization and robustness to perturbations compared to previous methods. Hirofumi et al. [8] conducted attribution work leveraging the latent recovery capability of GAN-generated images, achieving good recovery results when the image to be attributed is generated by the source model. These studies assume that the candidate model pool is known, but in reality, the image to be attributed may come from an unknown model. To address the open-set model attribution task, Yang et al. [30] pioneered a progressive open-space expansion method, gradually simulating open-set samples through a set of lightweight data augmentation models. With the rise of large-scale text-based image models, attribution research for text-based image models has begun. In addition, some work focuses on passive attribution research for deepfakes. Fernandes et al. [5] proposed a method for detecting deepfake videos based on an attribution confidence metric, without requiring access to training data or training calibration models on validation data. Considering that forged images may be generated by privately trained models, and the aforementioned work can only attribute specific generated images at the model level, Yang et al. [29] attempted to attribute forged images to the architecture of the source model, proposing the DNA-Det framework, which can successfully attribute images even if the source model is fine-tuned or retrained with different configurations. Jia et al. [9] explored the differences between deepfake videos generated by different models using a method based on spatial and temporal attention. To fully explore the hidden forgery traces in open-world unlabeled faces, Sun et al. [24] specifically proposed the CPL framework, guiding the feature alignment of manipulated facial regions by introducing a global-local voting module and designing a confidence-based soft pseudo-label strategy to mitigate pseudo-noise caused by similar methods in the unlabeled set.

As far as we know, there is only one study on the AIGC attribution of text-to-image generation models, i.e., DE-FAKE [22], which has been proposed to attribute fake images produced by text-to-image generative models. It focuses on four models: Stable Diffusion, Latent Diffusion, GLIDE, and DALL-E 2. By taking the correspondence of the images and

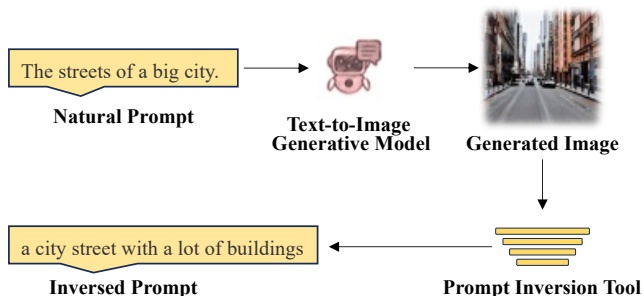


Figure 2: The schematic diagram of prompt inversion procedure.

prompts, DE-FAKE trains an attribution classifier, yielding impressive attribution performance. However, as larger text-to-image generative models emerge, it becomes impractical to enumerate all existing models for attribution. When a new model comes, DE-FAKE needs to re-train the model for better attribution. Hence, this method is not suitable for open-set attribution in real-world scenarios. Besides, the increasing number of potential models will contribute to the computation resource consumption. As a result, it is crucial to develop an attributor that can generalize to other generative models with high effectiveness and efficiency. In this paper, we aim to fill the gap. We propose a training-free attribution method, which takes advantage of the advanced prompt reconstructing and feature extracting tools, and can yield comparable attribution performance with the SOTA methods. It’s worth mentioning that our approach does not limit the number of models to be traced, hence perfectly adapted to the open-world AIGC attribution problem. The contributions are as follows:

- We design a training-free attribution framework, which contains textual prompt inversion, candidate image pool generation, similarity calculation, and ranking-based source inference modules.
- We analyze in detail the factors that can affect the effectiveness of traceability.
- Empirical experimental results highlight the effectiveness and the scalability of the proposed method, and also demonstrate the method’s robustness to resist common image processing attacks.

## 2 PRELIMINARIES

As we focus on the attribution of images generated by text-to-image generative models, in this section, we first introduce the models we consider in this work. Afterward, since our method needs to get the textual prompt for the test image, we list current common tools used for the inversion of the textual prompt.

### 2.1 Text-to-Image Generative Models

In recent years, there has been a growing interest in text-to-image generative models. These models typically take a piece

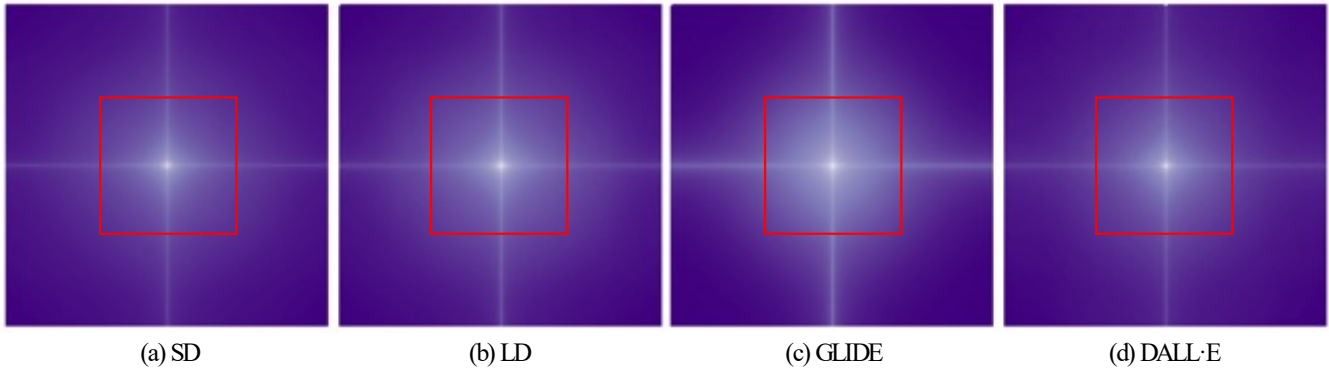


Figure 3: The magnitude spectra for fake images generated by text-to-image generative models (a) SD, (b) LD, (c) GLIDE, and (d) DALL-E, respectively. The high-frequency components are in the center, the low-frequency components distributed around.

of text (hard prompt) and random noise as input, and then use the prompt to guide the denoising process to generate an image that matches the prompt. This study specifically examines four widely available text-to-image generation models.

- Stable Diffusion [20]. Stable Diffusion (SD) is a text-to-image generation diffusion model. The model we use<sup>1</sup> is SD v1.5 which was initialized with the weights of the Stable-Diffusion-v1-2 checkpoint and subsequently fine-tuned on 595k steps at resolution 512x512 on “laion-aesthetics v2 5+”<sup>2</sup> and 10% dropping of the text-conditioning to improve classifier-free guidance sampling. Note that we refer to SD v1.5 as SD in the rest of our paper.
- Latent Diffusion [20]. Latent Diffusion (LD) is also a text-to-image generation diffusion model. The model we use<sup>3</sup> is the model pre-trained on LAION-400M [21]. Both SD and LD use the text encoders of CLIP [17] to guide the generation direction of fake models. Note that we refer to Latent Diffusion as LD in the rest of our paper.
- GLIDE [15]. GLIDE is a text-to-image generation model developed by OpenAI. The model we use<sup>4</sup> is trained on a filtered dataset containing hundreds of millions of text-image pairs. It’s worth noting that GLIDE may not perform well with prompts related to “person” topics, as images of people have been excluded from the training dataset due to ethical considerations.
- DALL-E mini [3]. DALL-E mini is a lightweight version of DALL-E [19], which is developed by researchers from Google and Huggingface. The model we use<sup>5</sup> adopts pre-trained VQGAN [4], BART [10], and CLIP [17] for training on total 15M prompt-image pairs. Considering the generation efficiency, we use DALL-E

mini to generate images rather than DALL-E [19] or DALL-E 2 [18]. Note that in the rest of this paper, we refer to DALL-E min as DALL-E.

## 2.2 Textual Prompt Inversion

In our method, we adopt the textual prompt of the test image as an important pivot to assist the attribution. That is, given an image, we need to reconstruct the prompt used to generate it. The procedure is displayed in Figure 2. Next, we will briefly introduce the relevant textual prompt inversion tools as below. Textual Prompt inversion, also known as hard prompt reconstruction, aims to inverse the textual prompt of AI-generated images. Different from embedding inversion methods [6, 25], textual prompt inversion aims to directly generate interpretable and readable textual prompts that can serve as the input.

Current textual prompt inversion methods can be mainly divided into three categories. The first approach is image captioning-based. By inputting the generated image into an image captioning model (e.g., ClipCap [14] and BLIP [11]) this approach considers the predicted caption as the prompt. Since the crucial prompt modifiers are absent in the caption, this approach cannot yield satisfactory results. The second approach is optimization-based. Take CLIP Interrogator [1] for instance, with a huge set of modifiers, it iteratively computes the similarity score between different combinations of modifiers and the given image. Once the similarity growth plateaus, the current combination is considered the predicted prompt. However, this approach suffers from low efficiency due to its design and relies on numerous manually defined hyper-parameters, potentially limiting its real-world applicability. The third category is learning-based. Shen et al. [23] first divide the prompt into subject and modifiers. On this basis, they adopt an image captioning model to obtain the subject and design a multi-label classifier to get modifiers. By concatenating the subject and the modifiers, they can inverse the prompt. Wen et al. [27] It optimizes the hard prompts using CLIP similarity between the image and text encodings from the CLIP encoders [17]. To address the

<sup>1</sup><https://huggingface.co/runwayml/stable-diffusion-v1-5>

<sup>2</sup><https://laion.ai/blog/laion-aesthetics/>

<sup>3</sup><https://github.com/CompVis/latent-diffusion>

<sup>4</sup><https://github.com/openai/glide-text2im>

<sup>5</sup><https://github.com/borisdayma/dalle-mini>

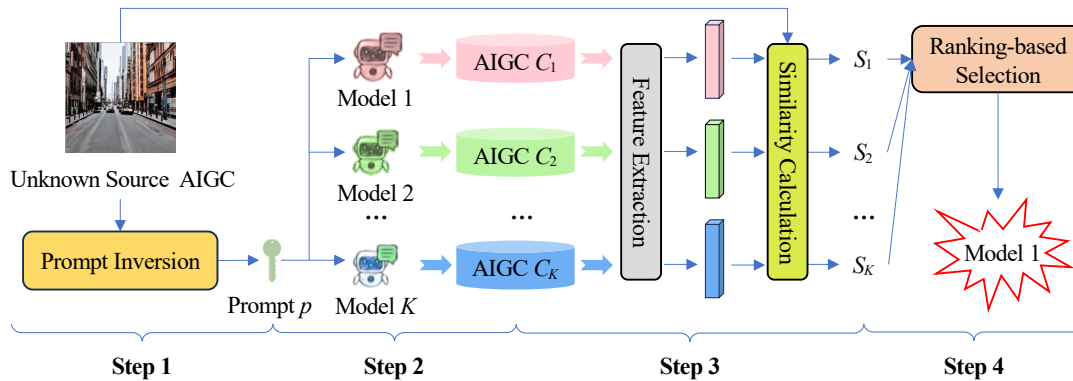


Figure 4: The framework of the proposed attribution method, which contains four steps: (1) Textual Prompt Inversion; (2) Candidate Image Pool Generation; (3) Similarity Calculation, and (4) Ranking-based Source Inference.

challenge posed by the fundamentally discrete nature of the resulting optimization problem and the exponentially large space of prompts, Mahajan et al. [13] use a delayed projection method to optimize prompts that represent the vocabulary space in the model. Additionally, they exploit the discovery that various stages of the diffusion process correspond to different levels of detail in an image. The later, noisier stages of the forward diffusion process relate to semantic information, so inverting the prompt in this range yields tokens that represent the image semantics.

### 3 THE PROPOSED METHOD

In this section, we first define the AI-generated image attribution task. Then, we analyze the distinguishability of images generated by different text-to-image generative models in the frequency domain. Finally, we briefly introduce the pipeline of the proposed method.

#### 3.1 Problem Definition & Analysis

Suppose we already know that the image is a fake image generated by a generative model. What we want to do now is confirm which model the image is generated by. We define the task as “AI-generated image attribution”. The conditions we have for attribution are as follows:

- A fake image to be attributed, denoted as  $I$ . The only thing we know about  $I$  is that it was generated by a text-to-image generative model.
- A group of candidate text-to-image generative models available for generation, denoted as  $ModelSet = \{M_1, M_2, \dots, M_K\}$ . Note that the size of  $ModelSet$ , i.e.,  $K$  is not a fixed value, as more and more text-to-image generative models are emerging nowadays.

We hold the belief that with the same prompt, images generated by the identical model tend to be more similar. Based on this belief, we design our method. As we aim to complete the above attribution procedure as efficiently as possible, we have abandoned the previous method of training neural networks to obtain classifiers for traceability. Instead, we make use of the distance information between image

pairs, and look for advanced similarity calculation methods to measure the distances. By doing so, we can infer the origin of the fake test image.

**Discussion** To demonstrate the distinguishability between different-source AI-generated fake images, we calculate the average of Fourier transform outputs of 1000 test images from each generative model respectively and visualize the frequency magnitude spectra in Figure 3. We can notice a small variation in the frequency spectra of fake images produced by different text-to-image generative models. Specifically, the central areas of the images exhibit greater brightness and more focused frequency spectra. This finding confirms the presence of a common latent feature in fake images generated by diverse text-to-image generative models.

Additionally, we visualize the radially averaged power spectra (RAPS)<sup>6</sup> for corresponding fake images in Figure 5. Consistent with Figure 3, the high-frequency components of the different source images are similar, with more pronounced differences in the low-frequency components. As displayed, the RAPS of fake images from different sources exhibit large differences. Among them, the GLIDE-generated images differ most from the other models, followed by LD. Besides, the spectra of the SD-generated images and DALL-E-generated images are harder to distinguish. Despite that small gap, our method can still achieve comparable accuracy in attributing fake images, showing the effectiveness of our proposed method.

#### 3.2 The Overall Framework

Figure 4 illustrates the whole framework of the proposed method, which consists of a total of four modules: (1) textual prompt inversion; (2) candidate image pool generation; (3) similarity calculation, and (4) ranking-based source inference.

<sup>6</sup>The radially averaged power spectrum (RAPS) is obtained by averaging the power spectrum over concentric circles centered at the origin (0 frequency) of the 2D power spectrum. RAPS is particularly useful when the direction of the frequency is not important, and we are only interested in the magnitude of the frequency components. It provides a 1D function that represents the distribution of power as a function of frequency magnitude, regardless of the direction.

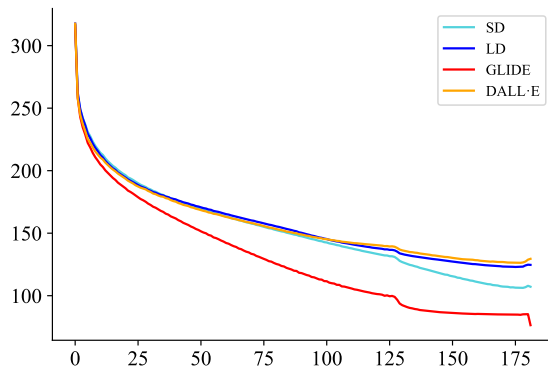


Figure 5: The visualization of radially averaged power spectra for fake images generated by various text-to-image generative models, respectively.

Among them, textual prompt inversion is the preliminary step. As the core of the proposed method is the similarity comparison between the test image and candidate images, how to generate high-quality relevant candidate images turns out to be an essential problem. To achieve this goal, we need to know the initial prompts of the test images. Ideally, we can get access to the initial prompts. However, under conditions that the initial prompts are not available, we need to find an alternative method to obtain prompts words that are functionally similar to the original prompts, which is what the prompt inversion step does in our method. After getting the functionally similar prompt, we input the inversed prompt into each candidate text-to-image model to regenerate a batch of images. These images are viewed as reference for subsequent attribution steps, called candidate images. With the test image and the candidate images generated from each model, we can inference the source models of the test image according to the similarity information. We pick a model as the source model if it can generate candidate images that are most similar to the test image.

The whole procedure is illustrated in Algorithm 1. In Section 4 and Section 5, we elaborate on each module of the proposed method orderly, and meanwhile clarify the feasibility.

## 4 CANDIDATE IMAGE REGENERATION

The first step of our method is to regenerate a set of candidate images. Therefore, we need to know the textual prompt that can generate the test image in advance. In this section, we consider two situations: (1) The initial prompt is available. (2) The initial prompt is unknown. The former situation is ideal, while in most cases, the prompt is unavailable. In the latter situation, we use off-the-shelf tools to reconstruct prompts that are functionally similar to the initial prompts. In this section, we first present the prompt inversion procedure, and then describe the candidate image generation process.

---

### Algorithm 1 The procedure of the attribution.

---

Input: The current test image  $I$ , A group of candidate models  $ModelSet = \{M_1, M_2, \dots, M_K\}$   
 Output: Source model  $M_{best}$   
 1:  $F_I \leftarrow FeatureExtrate(I)$   
 2:  $prompt\ p \leftarrow PromptInverse(I)$   
 3: for  $k \leftarrow 1$  to  $K$  do  
 4:  $ImageSet_k \leftarrow CandidatePoolGenerate(prompt, M_k)$   
 5:  $FeatureSet_k \leftarrow FeatureExtrate(ImageSet_k)$   
 6:  $SimScoreSet_k \leftarrow SimilarityCalculate(F_I, FeatureSet_k)$   
 7:  $Score_k \leftarrow Rank(SimScoreSet_k)$   
 8: end for  
 9:  $ScoreSets \leftarrow \{Score_1, Score_2, \dots, Score_K\}$   
 10:  $M_{best} \leftarrow argmax(ScoreSets)$

---

Table 1: The similarity of natural prompts and prompts generated by different inversion tools.

Prompt Inversion Tool	Noun	Verb	Total
PEZ [28]	0.0210	0.0059	0.0110
BLIP [11]	0.2100	0.1009	0.1678

### 4.1 Textual Prompt Inversion

For the current test image  $I$ , we first need to obtain the original textual prompt  $p$  used to generate  $I$ . In this step, we consider two conditions: (1) The prompt is known; (2) The prompt is unknown. For condition (1), we have the identical prompt used to generate the current image  $I$ ; for condition (2), we have no access to the initial prompt for generating  $I$ . In this case, we use a prompt inversion tool to generate an alternative prompt. Here we adopt an image captioning model to generate a caption as the alternative prompt. We call the prompt in condition (1) as Natural Prompt and the alternative prompt in condition (2) as Generated Prompt. In the following pages, the prompts mentioned are textual prompts by default.

Feasibility Analysis Figure 6 displays some examples of test images produced by various text-to-image generative models and their corresponding prompts, including the initial natural prompt from Flickr30k [16] dataset and the generated prompts inversed via BLIP [11] and PEZ [28], respectively. Accordingly, compared to PEZ, BLIP can inverse prompts that are more relevant to the natural prompt with higher readability. What’s more, the objects (e.g., city, street, van, and man) and actions (e.g., sitting) can be inversed accurately, demonstrating the descriptive ability of BLIP. In contrast, PEZ fails to achieve the above result, and the prompts it generates are mostly meaningless combinations of low-frequency tokens. To more objectively compare the two methods, we calculate the similarity of natural prompts and prompts generated by BLIP and PEZ <sup>7</sup>, respectively.

<sup>7</sup>We use the NLTK toolkit (<https://www.nltk.org/>) i.e., `word_tokenize` and `pos_tag`, to complete calculation on all the test samples







	<b>Natural Prompt:</b> The <b>streets</b> of a big <b>city</b> . <b>Prompt Generated by BLIP:</b> a <b>city street</b> with a lot of buildings <b>Prompt Inversed by PEZ:</b> expanse lessly frightening empty newyorkcity <b>straightstreets</b> lush — flirting dissent quote♥ equities encroless
	<b>Natural Prompt:</b> A car and a <b>minivan</b> have collided. <b>Prompt Generated by BLIP:</b> a <b>van</b> is parked in a field of grass <b>Prompt Inversed by PEZ:</b> Jbloggdatabases huge toyota sprahi wagon stored massachsurvecrashed in thaitaxi
	<b>Natural Prompt:</b> A man is going to cut-up a chicken for cooking. <b>Prompt Generated by BLIP:</b> a close up of a plate of food with shrimp <b>Prompt Inversed by PEZ:</b> ~! novascototheres horus pretzel dough lapse – ♥♥ novascopanda pr figurine tasty fishy
	<b>Natural Prompt:</b> A <b>man</b> is <b>sitting</b> behind a hard wood counter. <b>Prompt Generated by BLIP:</b> a <b>man sitting</b> on a bench in a library <b>Prompt Inversed by PEZ:</b> wickedkitchen transformed carmel berkshire spraying safardrexhartman photoshop rendering shown shabby luv pixar acidity

Figure 6: Illustration of AI-generated images and corresponding prompts, where the natural prompts are the initial prompts used to generate the test image in the same row. We highlight the words that appear both in natural prompts (in green) and prompts inversed by BLIP (in blue) or PEZ (in purple).

















































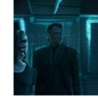

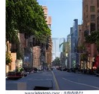








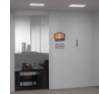

<b>Test Image</b> 					<b>Prompt Generated by BLIP:</b> a city street with a lot of buildings				<b>Prompt Inversed by PEZ:</b> expanse lessly frightening empty newyorkcity straightstreets lush — flirting dissent quote♥ equities encroless			
<b>Natural Prompt:</b> The streets of a big city.	<b>SD</b>	<b>LD</b>	<b>GLIDE</b>	<b>DALL-E</b>	<b>SD</b>	<b>LD</b>	<b>GLIDE</b>	<b>DALL-E</b>	<b>SD</b>	<b>LD</b>	<b>GLIDE</b>	<b>DALL-E</b>
												
												
												
												
												

Figure 7: Illustration of images generated by various models using different prompts.

From Table 1, we can see that compared to the prompt generated by PEZ, the prompts generated by BLIP are more similar to natural prompts at the word level. Hence in later

experiments, we adopt BLIP rather than PEZ as the prompt inversion tool.

## 4.2 Candidate Image Pool Generation

Afterward, we put the obtained prompt  $p$  into every text-to-image generative model  $M_k$  to generate  $\gamma$  candidate images  $ImageSet_k$  ( $k \in \{1, 2, \dots, K\}$ , respectively, where  $K$  is the total number of candidate models. Then we get a candidate image pool consisting of  $K$  image sets, totally  $\gamma * K$  candidate images. Note that  $\gamma$  is a pre-defined hyper-parameter.

**Feasibility Analysis** Given a test image, we separately input the corresponding natural prompt, prompt inverted by BLIP, and prompt inverted by PEZ into each candidate text-to-image generative model to generate candidate images. Figure 7 gives some examples of the images generated by different models, respectively. As displayed, both the natural prompt and the BLIP-generated prompt can induce all of the four generative models to produce semantically relevant images, which benefits the attribution performance, while for prompt generated by PEZ [28], it can only trigger the SD model to generate semantically and highly relevant images with the test image. This directly leads to low accuracy in test images generated by text-to-image generative models other than SD, as we will discuss in Section 6.6. This phenomenon also suggests that, even if the prompts are not readable by humans, they can still generate high-quality images. The referentiality of candidate images lays the foundation for the proposed attribution method.

Another interesting phenomenon we can discover is that the generative models are capable of generating contents that don't exist in the prompt, such as people on the street. This phenomenon is particularly obvious for the SD model, as we observe people in all the prompt conditions from Figure 7.

## 5 SIMILARITY BASED INFERENCE

After steps in Section 4, we get a set of candidate images from various models. Next, we aim to use these regenerated images to complete the inference. In this section, we first point out how we calculate the similarity between the test image and the candidate images, and then we present how to inference the source model depending on the calculated similarity scores.

### 5.1 Similarity Calculation

Next, we measure the similarity of  $I$  with  $ImageSet_k$  ( $k \in \{1, 2, \dots, K\}$ ). We first use a well-performed feature extractor to get feature representations of image  $I$  and  $\gamma * K$  candidate images, i.e.,  $F_I$ , and  $FeatureSet_k$  ( $k \in \{1, 2, \dots, K\}$ ). Then, we calculate the similarity score of  $F_I$  and  $FeatureSet_k$  separately, i.e.,

$$SimScoreSet_k = [func(F_I, FeatureSet_1^k), \dots, func(F_I, FeatureSet_\gamma^k)]$$

$$func(F_I, FeatureSet_i^k) = \frac{F_I \cdot FeatureSet_i^k}{|F_I| |FeatureSet_i^k|}, \quad (1)$$

where  $SimScoreSet_k$  contains  $\gamma$  values, each value indicating the similarity score of image  $I$  with the  $i$ -th image  $FeatureSet_i^k$

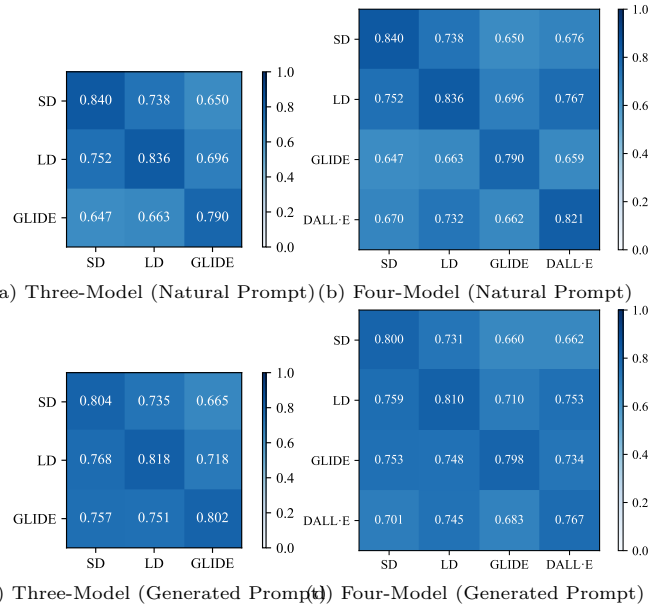


Figure 8: The visualization of similarity matrices under different attribution scenarios. Each row in the matrix represents the similarity scores between images generated by the current text-to-image generative model and each candidate model.

in  $ImageSet_k$ ;  $func(\cdot)$  represents cosine similarity calculation function.

**Feasibility Analysis** According to Figure 8, in all the conditions, the values on the diagonals are significantly higher than the other values. For example, in Figure 8 (a), the SD-generated test images have a value of 0.840 similarity with SD-generated images, while only have a value of 0.650 similarity with GLIDE-generated image. This phenomenon indicates that images generated from identical models tend to be more similar. Note that even with the information loss caused by the prompt inversion module (refer to Figure 8 (c) and Figure 8 (d)), images generated from the same model still have the highest similarity, which coincides with the principle of the proposed method.

### 5.2 Ranking-based Inference

After Step 3, we get  $\gamma * K$  similarity scores, i.e.,  $SimScoreSet_k$  ( $k \in \{1, 2, \dots, K\}$ ). In this step, we calculate a final score  $Score_k$  for each candidate model  $k$  and rank the candidate models according to these final scores. Here, we design three ranking schemes for the final score calculation.

1. AVG: Calculate the average similarity score of  $SimScoreSet_k$ , i.e.,  $mean(SimScoreSet_k)$ .
2. BEST: Choose the highest similarity score of  $SimScoreSet_k$ , i.e.,  $max(SimScoreSet_k)$ .
3. AVG+BEST: Get the mean value of the average score and highest score, i.e.,  $\frac{mean(SimScoreSet_k) + max(SimScoreSet_k)}{2}$ .

After the above procedure, by sorting the final scores in descending order, we can pick the highest-ranked model as the source of image  $I$ .

## 6 EXPERIMENTAL RESULTS

In this section, we first introduce the experimental settings and evaluation metrics, and then we experimentally validate the effectiveness, scalability and robustness of the proposed approach. Besides, since our method does not require training, we argue the usability of our method on efficiency. Finally, we demonstrate the effectiveness of the individual modules in the proposed method through extensive ablation experiments.

### 6.1 Experimental Settings

We describe the configuration of the experiment, including text-to-image generative models, baselines and datasets, as well as the implementation details.

**Text-to-Image Generative Models** We use four popular pre-trained text-to-image generative models, i.e., Stable Diffusion v1.5 (SD for short) [20], Latent Diffusion (LD for short) [20], GLIDE [15], and DALL-E mini (DALL-E for short) [3], for experiments. The resolution of the images generated by SD is  $512 * 512$ , and  $256 * 256$  for the other three models.

**Baselines & Datasets** We use the most related state-of-the-art work DE-FAKE [22] as the baseline, which also focuses on attributing AIGC by text-to-image generative models. To evaluate the scalability ability of DE-FAKE, we randomly take 20,000 captions from MSCOCO [12] dataset as training prompts and 1,000 captions from Flickr30k [16] dataset as natural test prompts to produce fake images for different generative models. Finally, we get 80000 fake images for training and validation, and 4,000 fake images for testing, with 1,000 test images for each text-to-image generative model.

As our method doesn’t require a training dataset, we only need to construct a test set. We use the same test set with DE-FAKE for fair comparison. Figure 9 displays some test images using captions from Flickr30k [16].

**Implementation Details** We use BLIP [11] as the caption generation model for both DE-FAKE and the proposed method. We use CLIP [17] for image feature extraction. The default value of  $\gamma$  is fixed as 100. We use an NVIDIA H800 PCIe GPU for calculation and the random seed is 2023.

### 6.2 Evaluation Metrics

We use accuracy (Acc), Recall, Precision, as well as F1 Score to evaluate the performance of the proposed method, in which accuracy is used to evaluate the method’s attribution performance on the whole test set, and the other three metrics are used to reflect how well the method performs on images generated by a specific generative model.

**Accuracy** Given a test set with images generated by different text-to-image generative models, the Accuracy (Acc) reflects how accurately the method predicts the source model in the whole. The value of accuracy is calculated as follows:

$$Acc = \frac{1}{N} \sum_{i=1}^N (Y_p^i = Y_t^i), \quad (2)$$

where  $Y_p^i$  and  $Y_t^i$  are the predicted label and ground-truth label of the  $i$ -th image, respectively;  $N$  denotes the total number of images to be attributed.

**Recall** This metric measures the ability of the method to find all the relevant images produced by a specific model  $M_k$  (e.g., the SD model). It calculates the ratio of the number of images correctly predicted as  $M_k$  to the number of images whose ground-truth label is  $M_k$ , i.e.,

$$Recall = \frac{\sum_{i=1}^N Y_p^i = Y_t^i = M_k}{\sum_{i=1}^N Y_t^i = M_k}. \quad (3)$$

**Precision** This metric measures the ability of the method to identify only the relevant images produced by a specific model  $M_k$  (e.g., the SD model). It calculates the ratio of the number of images correctly predicted as  $M_k$  to the number of all the images predicted as  $M_k$ , i.e.,

$$Precision = \frac{\sum_{i=1}^N Y_p^i = Y_t^i = M_k}{\sum_{i=1}^N Y_p^i = M_k}. \quad (4)$$

**F1 Score** This metric is the harmonic mean of Recall and Precision, i.e.,

$$F1 = \frac{2 \times Recall \times Precision}{Recall + Precision}. \quad (5)$$

Among all the metrics above, higher values indicate better performance.

### 6.3 Comparison with SOTA

To better evaluate the scalability of the proposed methods, we consider both three-model attribution and four-model attribution scenarios. Note that for DE-FAKE, we re-train it to adapt to the four-model attribution scenario. Table 2 and Table 3 give the attribution performance of different methods. Overall, our proposed method can achieve comparable performance with DE-FAKE on both three-model attribution and four-model attribution scenarios. Concretely, in the three-model (four-model) attribution scenario, the average accuracy reaches 97.23% (94.13%) and 88.23% (79.90%) for natural prompt condition and generated prompts condition, respectively. What’s more, we can also observe that in the natural prompt condition, the attribution performance on each generative model is relatively similar. While in the generated prompt condition, the attribution performance on the fake images from different source models varies to a large extent. For example, in the four-model attribution scenario with generated prompts, the images generated by the SD model have a rather high attribution accuracy (i.e., 0.911%), while the images generated by DALL-E tend to be more difficult to attribute, with the attribution accuracy reaching only 0.689%.



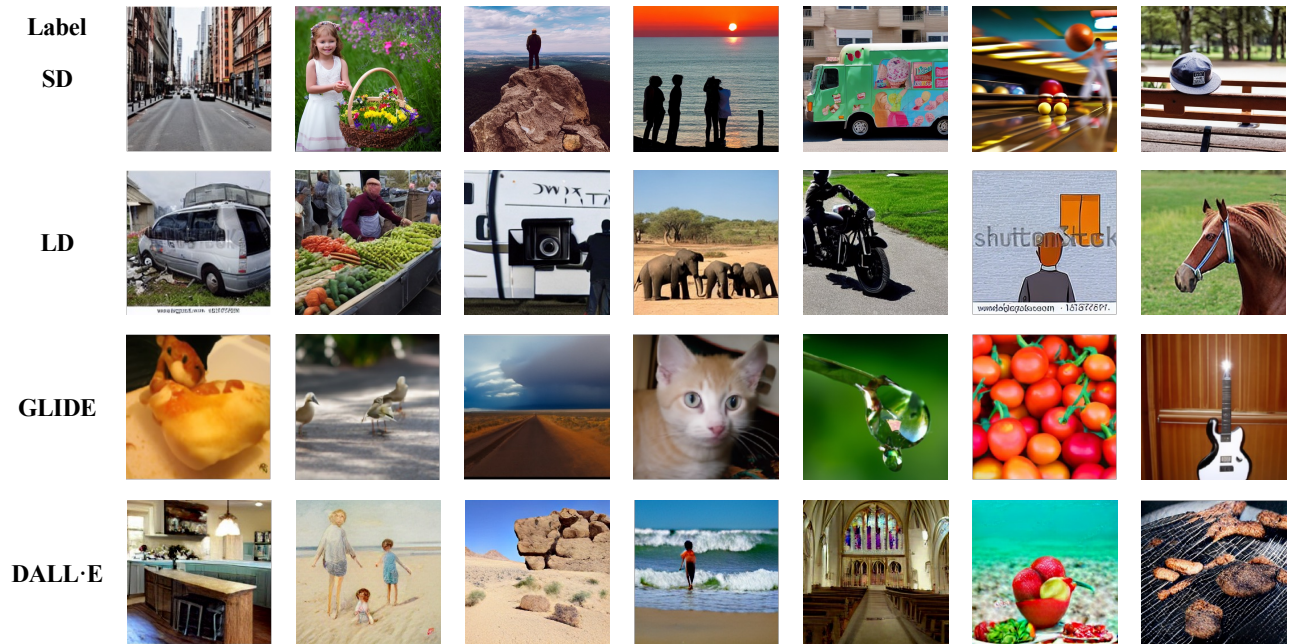


Figure 9: Selected examples of test images generated using prompts from Flickr30k [16].

Table 2: The comparison of the three-model attribution performance among different methods.

Method	Acc	Recall			Precision			F1 Score		
		SD	LD	GLIDE	SD	LD	GLIDE	SD	LD	GLIDE
DE-FAKE (Image-Only)	80.50	0.839	0.643	0.933	0.710	0.786	0.933	0.769	0.707	0.933
DE-FAKE (Natural Prompt)	95.67	0.949	0.930	0.991	0.933	0.939	0.998	0.941	0.935	0.995
DE-FAKE (Generated Prompt)	94.83	0.932	0.925	0.988	0.926	0.921	0.998	0.929	0.923	0.993
Proposed (Natural Prompt, $\gamma = 20$ )	97.23	0.989	0.942	0.986	0.947	0.979	0.992	0.968	0.960	0.989
Proposed (Generated Prompt, $\gamma = 100$ )	88.23	0.925	0.835	0.887	0.825	0.889	0.944	0.872	0.861	0.914

Table 3: The comparison of the four-model attribution performance among different methods.

Method	Acc	Recall				Precision				F1 Score			
		SD	LD	GLIDE	DALL·E	SD	LD	GLIDE	DALL·E	SD	LD	GLIDE	DALL·E
DE-FAKE (Image-Only)	62.15	0.931	0.288	0.712	0.555	0.474	0.641	0.957	0.660	0.628	0.398	0.817	0.603
DE-FAKE (Natural Prompt)	95.23	0.940	0.910	0.991	0.968	0.931	0.909	0.995	0.975	0.935	0.910	0.993	0.971
DE-FAKE (Generated Prompt)	94.68	0.921	0.892	0.987	0.987	0.907	0.909	0.995	0.976	0.914	0.901	0.991	0.982
Proposed (Natural Prompt, $\gamma = 20$ )	95.70	0.988	0.895	0.978	0.928	0.946	0.964	0.982	0.938	0.966	0.928	0.980	0.952
Proposed (Generated Prompt, $\gamma = 50$ )	79.90	0.911	0.755	0.841	0.689	0.788	0.699	0.908	0.822	0.845	0.726	0.873	0.750

Table 4: Robustness evaluation for the AIGC attribution. The optimal results are shown in bold, and the second-best results are indicated with \*.

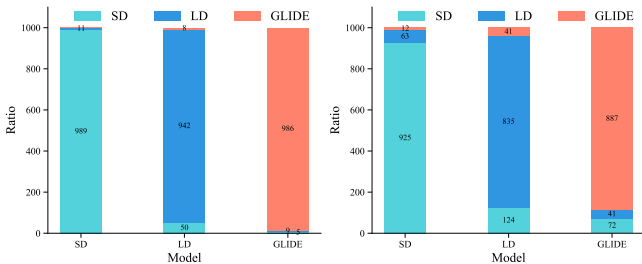
Method	Three-Attribution				Four-Attribution			
	Gaussian Blurring	JPEG Compression	Resizing	Avg.	Gaussian Blurring	JPEG Compression	Resizing	Avg.
DE-FAKE (Image-Only)	69.07	83.07	74.83	75.66	66.88	65.15	75.50	69.18
DE-FAKE (Natural Prompt)	68.60	90.90	70.10	76.53	52.43	88.33	53.28	64.68
DE-FAKE (Generated Prompt)	72.37	89.40	74.03	78.60	51.83	84.98	53.03	63.28
Proposed (Natural Prompt) <sup>1</sup>	92.57	95.27	90.70	92.85	88.83	93.80	84.70	89.11
Proposed (Generated Prompt) <sup>2</sup>	82.57*	82.77	78.50*	81.28*	69.70*	74.43	65.28	69.80*

<sup>1</sup> We set  $\gamma = 20$  for both the three-model attribution and the four-model attribution, respectively.

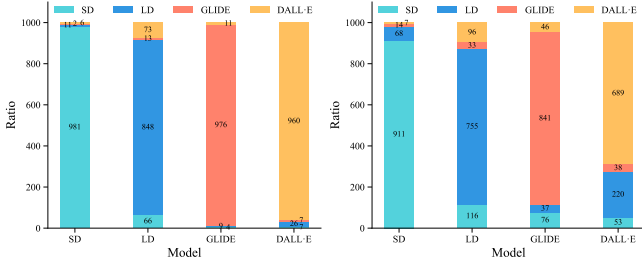
<sup>2</sup> We set  $\gamma = 100$  for the three-model attribution and  $\gamma = 50$  for the four-model attribution, respectively.

**Inter-class Confusion** We also visualize the value of Recall for each generative model. The results are depicted in Figure 10.

As displayed, images generated by the SD and LD models are



(a) Proposed (Natural Prompt) (b) Proposed (Generated Prompt)



(c) Proposed (Natural Prompt) (d) Proposed (Generated Prompt)

Figure 10: The visualization of confusion matrices for each model. The first row shows three-model attribution; the second row shows four-model attribution.

easily confused with each other. This is explainable, as Figure 3 shows these two models’ frequency spectra are more similar. Besides, the DALL-E-generated images are more likely to be incorrectly attributed as LD and vice versa, corroborating the analysis in Figure 5. We can also get the conclusion in Figure 8 that compared to GLIDE, DALL-E produces images more similar to those of SD and LD. This partly hinders our proposed traceability method based on similarity measures.

### 6.4 Robustness Analysis

To evaluate the robustness of the proposed method, we take three common image process methods as attack operations, i.e., (1) Gaussian blurring ( $\sigma = 1.0$ ), (2) JPEG compression ( $QF = 0.95$ ), and (3) Resizing ( $scale = 0.5$ )<sup>8</sup>. For all the test images, we proceed with the three attack methods to get corresponding attacked images, respectively.

Table 4 shows the attribution results under the three attack scenarios above. As highlighted, in the Natural Prompt condition where the prompts are known, our proposed method can outperform DE-FAKE in all three attack scenarios. Besides, even in the Generated Prompt condition, our method can still acquire good traceability results comprehensively. The reason, on the one hand, is credited to the powerful descriptive ability of BLIP to interpret images, and on the other hand, is due to the appropriate selection of the similarity calculation function. Concretely, our method is essentially based on the measure of semantic similarity, which uses the

<sup>8</sup>We scale each image to half of its original size. For SD-generated images, the size becomes  $256 \times 256$ , and for images produced by other models, the size becomes  $128 \times 128$ .

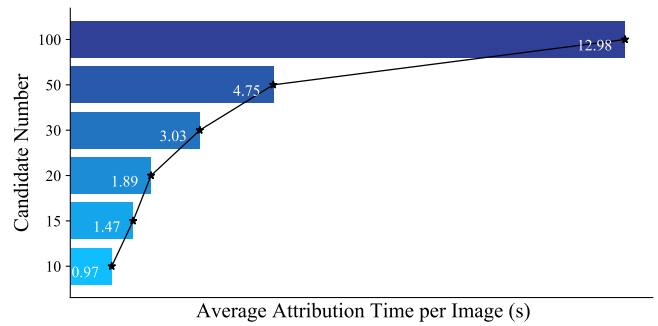


Figure 11: Trade-off between attribution performance and efficiency. (Testing procedure for Three-Model Attribution)

Table 5: The time cost of the three-model attribution with different methods.

Method	Training Time	Test Time (Per Sample)
DE-FAKE (Image-Only)	45h+	<0.05s
DE-FAKE (Natural Prompt)	45h+	<0.05s
DE-FAKE (Generated Prompt)	45h+	<0.05s
Proposed (Natural Prompt)	0	~ 3s ( $\gamma = 30$ )
Proposed (Generated Prompt)	0	~ 3s ( $\gamma = 30$ )

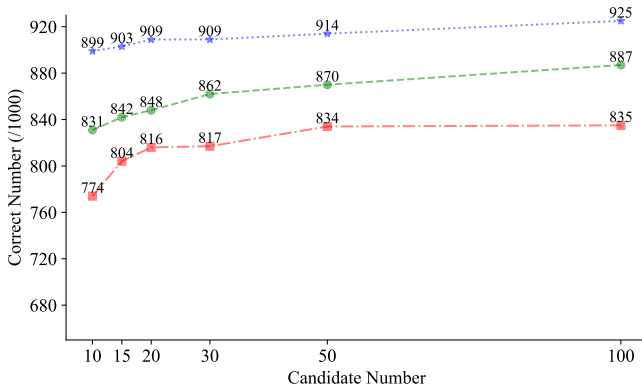
semantic features extracted by CLIP as the basis for similarity calculation, so it has high robustness to attack methods that aim to erase image textures, e.g., Gaussian blurring. In summary, this experiment demonstrates the satisfactory robustness of the proposed method.

### 6.5 Attribution Efficiency

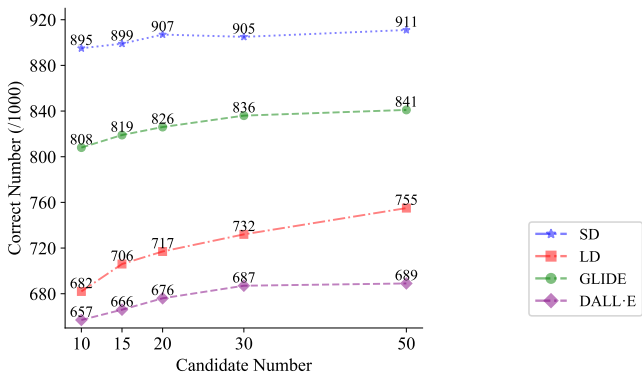
As we have mentioned before, our method doesn’t need any training procedure, i.e., training-free, which saves time to a large extent. Table 5 compares the attribution time for DE-FAKE [22] and our proposed method under the same experimental conditions. As can be seen, compared with DE-FAKE, the proposed method does not require training, which greatly saves the time cost for attribution. At the same time, on the premise of accuracy, the attribution efficiency during the test stage is also within an acceptable range. Note that there exists a trade-off between the attribution accuracy and efficiency. Theoretically, the more candidate images, the better the attribution performance, yet at the price of sacrificing efficiency. Experimentally, with the increasing number of candidate images, the accuracy improves (Figure 12 and Table 7), while the time for attributing also increases (Figure 11). When the number of candidate images reaches 100, the time to attribute an image using the proposed method is about 13 seconds.

### 6.6 Ablation Study

In this section, we explore how several important modules influence the final attribution performance. We conduct all the ablation studies in the three-model attribution scenario.



(a) Three-Model Attribution (Generated Prompt)



(b) Four-Model Attribution (Generated Prompt)

Figure 12: The impact of candidate number on each model’s attribution performance.

 Table 6: The impact of different prompt inversion tools on the three-model attribution performance. ( $\gamma = 10$ )

Prompt Inversion Tool	SD	LD	GLIDE	Acc
Natural Prompt	0.982	0.915	0.985	96.07
BLIP [11]	0.899	0.774	0.831	83.47
PEZ [28]	0.965	0.243	0.456	55.47

**Prompt Inversion Tool** The first step of our method is to obtain the prompt of the test image. We want to see how the quality of the inversed prompt words affects the attribution results. Here we use BLIP [11] and PEZ [28] to conduct experiments.

Table 6 shows the attribution results from different prompt inversion tools. We can see that different prompt inversion tools lead to different attribution performance, and for different models, the attribution performance changes differently. For the SD model, PEZ outperforms BLIP, while for other models, vice versa. This is because the PEZ algorithm is specifically designed to get prompts from images generated by the SD model. Therefore, the corresponding results enjoy an increase. This verifies that the quality of the prompt can

Table 7: The impact of candidate number on the attribution performance.

Candidate Pool Scale ( $\gamma$ )	Three-Model Attribution	Four-Model Attribution
10	83.47	76.05
15	84.97	77.25
20	85.77	78.15
30	86.27	79.00
50	87.27	79.90
100	88.23	/

 Table 8: The impact of different similarity calculation methods on the three-model attribution performance. ( $\gamma = 100$ )

Similarity Calculation Method	SD	LD	GLIDE	Acc
CosCLIP [17]	0.925	0.835	0.887	88.23
SSIM [26]	0.620	0.600	0.912	34.47
CLIP+SSIM	0.840	0.628	0.946	80.47

 Table 9: The impact of different ranking schemes on the three-model attribution performance. ( $\gamma = 100$ )

Ranking Scheme	SD	LD	GLIDE	Acc
AVG	0.915	0.649	0.832	79.87
BEST	0.914	0.835	0.881	87.67
AVG+BEST	0.925	0.759	0.887	85.70

surely affect the attribution performance. In addition, we can observe from Table 2 and Table 3 that the proposed method with natural prompt ( $\gamma = 10$ ) performs better than prompts generated by BLIP ( $\gamma = 100$ ). This phenomenon tells us that as long as the inversed prompt is good enough, we can still reach a high attribution accuracy even using fewer candidate images.

**Candidate Pool Scale** With the inversed prompts, the next step is to generate candidate images. Table 7 shows the impact of the number of candidate images (i.e., the value of  $\gamma$  in Algorithm 1) on the whole attribution accuracy. Accordingly, as the number of candidate images increases, the attribution accuracy also rises, which shows that more candidate images lead to better attribution accuracy.

Figure 12 displays the impact of the number of candidate images on each model’s attribution performance separately. It indicates that different models exhibit different sensitivities to the value of  $\gamma$ . For example, the curve of the SD model changes relatively flat, indicating that the traceability accuracy of SD-generated content is less affected by the size of candidate images. In contrast, with the increasing value of  $\gamma$ , the LD curve changes significantly, suggesting the traceability of LD-generated content depends on the size of candidate images to a larger extent. Note that for the qua-attribution situation (Figure 12 (a)), when the value reaches 100, the growth rate of all curves slows down except for the LD model, which means that the LD traceability results can be further improved by increasing the size of the candidate images.

Table 10: Comparison of SOTA’s performance changes before and after data augment using the proposed method.

Models	Accuracy		Robustness			Avg. Boost
	No Attack	Gaussian Blurring	JPEG Compression	Resizing	Avg.	
DE-FAKE(Image-Only) (w/o aug)	80.53	69.07	83.07	74.83	75.66	-
DE-FAKE(Image-Only) (w/ aug)	79.67	69.60+0.53	80.77	77.73+2.90	76.03+0.38	+0.07
DE-FAKE(Natural Prompt) (w/o aug)	95.63	68.60	90.90	70.10	76.53	-
DE-FAKE(Natural Prompt) (w/ aug)	96.03+0.40	72.00+3.40	92.80+1.90	73.87+3.77	79.56+3.02	+1.72
DE-FAKE(Generated Prompt) (w/o aug)	94.87	72.37	89.40	74.03	78.60	-
DE-FAKE(Generated Prompt) (w/ aug)	95.13+0.26	74.80+2.43	90.67+1.27	76.10+2.07	80.52+1.92	+1.51

**Similarity Calculation Method** We use (1) CosCLIP: the cosine similarity score of features extracted by CLIP [17] and (2) SSIM: the Structural Similarity [26] score to evaluate the distance between image-pairs, respectively. Results from Table 8 show that the similarity calculation method makes a huge difference to the attribution result, and AIGC produced by different models exhibit different calculation preferences. For example, SSIM can better distinguish images generated by the GLIDE model (i.e., 0.912 for GLIDE), while it has little effect on identifying images generated by other models (i.e., 0.620 for SD and 0.600 for LD). In contrast, the ability of CosCLIP to recognize contents generated by different models is relatively balanced, with the Recall reaching 0.925, 0.835, and 0.887 for SD, LD, and GLIDE, respectively. What’s more, we combine CosCLIP and SSIM to see whether their combination can boost the attribution performance. It turns out that the combination of CosCLIP and SSIM works on GLIDE most significantly, with the value of Recall increasing by 3.4%.

**Ranking Scheme** After getting the similarity scores of the test image and all the candidate images, the final step is to select the source model accordingly. As described in Section 5.2, We design three ranking schemes for the source model selection. Table 9 gives comparisons of different ranking schemes. As can be seen, for SD and GLIDE models, the AVG+BEST ranking scheme performs best, and for the LD model, the BEST ranking scheme performs best. Therefore, we in the experiments take the most suitable ranking scheme for each model, respectively.

## 7 PROPOSED METHOD AS PLUG-IN

The previous sections have exhibited the effectiveness, scalability, as well as robustness of the proposed method. In this section, we explore whether our proposed method can work as a data augmentation tool to boost the performance of the existing training-based attribution method.

We experiment on the state-of-the-art method DE-FAKE [22]. As DE-FAKE is training-based, the way we assist it is to generate more training images through the first two steps of our method, i.e., (1) Textual Prompt Inversion and (2) Candidate Image Pool Generation. Concretely, for each image in the training set, we first use BLIP to obtain a caption as its prompt, and then we generate 10 images using the generative model corresponding to the ground-truth label of the current training image. This equates to a 10-fold expansion of the original training set. Afterward, we use the

augmented training set to retrain DE-FAKE and evaluate the model’s performance on the same testing set.

The experiment results are displayed in Table 10. As shown, after data augmenting with our method, both the accuracy and robustness of DE-FAKE enjoy different degrees of improvement. Among the three situations, DE-FAKE (Natural Prompt) shows the highest improvement, with the attribution accuracy and the average robustness indicator enhancing by 0.40% and 3.02%, respectively. In contrast, for DE-FAKE (Image-Only), the performance enhancement is not very obvious. We think this is because, in the Image-Only case, DE-FAKE fails to fully utilize the correlation between images and prompts, resulting in the data enhancement based on our method not being well facilitated. Nevertheless, the proposed method has led to an increase in robustness. These experiment results verify the compatibility and effectiveness of the proposed method as a means of data augmentation.

## 8 CONCLUSION

To tackle the problem of AI-generated image attribution, we propose a straightforward method to complete the attribution of fake images generated by text-to-image generative models to their source models. Instead of training a classifier as the previous methods do, we design a simple but effective training-free method. Given a test image, we first use the inversed prompts to produce candidate images. Afterward, by measuring the similarity distance between the test image and the candidate images, we select the source model according to the ranking-based scheme. Empirical results demonstrate that our method has exhibited satisfactory attribution performance on effectiveness, generalization ability, as well as robustness, and the high efficiency makes our method friendly to real-time and open-world traceability scenarios.

From ablation studies, we witness the importance of prompts on the whole attribution procedure. Therefore, how to get accurate hard prompts turns out to be an essential problem. In the future, we aim to design better prompt inversion methods, and improve the quality of the prompts inferred from the test images, hence enhancing the attribution accuracy. In addition, the similarity calculation method also plays an essential role in the attribution procedure. Therefore, how to devise the similarity calculation module according to the fingerprints left by different text-to-image generative models is worth exploring.

We hope this work can shed some light on the open-set AI-generated image attribution in the real world, and we



also expect this work can raise awareness of protecting the copyright of the text-to-image generative models.

## REFERENCES

- [1] [n. d.]. <https://github.com/pharmapsychotic/clip-interrogator>.
- [2] Tu Bui, Ning Yu, and John Collomosse. 2022. Repmix: Representation mixing for robust attribution of synthesized images. In European Conference on Computer Vision. Springer, 146–163.
- [3] Boris Dayma, Suraj Patil, Pedro Cuenca, Khalid Saifullah, Tanishq Abraham, Phúc Lê Khắc, Luke Melas, and Ritobrata Ghosh. 2021. DALL-E Mini. <https://doi.org/10.5281/zenodo.5146400>
- [4] Patrick Esser, Robin Rombach, and Bjorn Ommer. 2021. Taming transformers for high-resolution image synthesis. In Proceedings of the IEEE/CVF conference on computer vision and pattern recognition. 12873–12883.
- [5] Steven Fernandes, Sunny Raj, Rickard Ewetz, Jodh Singh Pannu, Sumit Kumar Jha, Eddy Ortiz, Iustina Vintila, and Margaret Salter. 2020. Detecting deepfake videos using attribution-based confidence metric. In Proceedings of the IEEE/CVF Conference on Computer Vision and Pattern Recognition Workshops. 308–309.
- [6] Rinon Gal, Yuval Alaluf, Yuval Atzmon, Or Patashnik, Amit Haim Bermano, Gal Chechik, and Daniel Cohen-Or. 2023. An Image is Worth One Word: Personalizing Text-to-Image Generation using Textual Inversion. In The Eleventh International Conference on Learning Representations, ICLR 2023, Kigali, Rwanda, May 1-5, 2023. OpenReview.net. <https://openreview.net/pdf?id=NAQvF08TcyG>
- [7] Sharath Girish, Saksham Suri, Sai Saketh Rambhatla, and Abhinav Shrivastava. 2021. Towards discovery and attribution of open-world gan generated images. In Proceedings of the IEEE/CVF International Conference on Computer Vision. 14094–14103.
- [8] Syou Hirofumi, Kazuto Fukuchi, Yohei Akimoto, and Jun Sakuma. 2022. Did You Use My GAN to Generate Fake? Post-hoc Attribution of GAN Generated Images via Latent Recovery. In 2022 International Joint Conference on Neural Networks (IJCNN). IEEE, 1–8.
- [9] Shan Jia, Xin Li, and Siwei Lyu. 2022. Model attribution of face-swap deepfake videos. In 2022 IEEE International Conference on Image Processing (ICIP). IEEE, 2356–2360.
- [10] Mike Lewis, Yinhan Liu, Naman Goyal, Marjan Ghazvininejad, Abdelrahman Mohamed, Omer Levy, Veselin Stoyanov, and Luke Zettlemoyer. 2020. BART: Denoising Sequence-to-Sequence Pre-training for Natural Language Generation, Translation, and Comprehension. In Proceedings of the 58th Annual Meeting of the Association for Computational Linguistics, ACL 2020, Online, July 5-10, 2020, Dan Jurafsky, Joyce Chai, Natalie Schluter, and Joel R. Tetraault (Eds.). Association for Computational Linguistics, 7871–7880. <https://doi.org/10.18653/V1/2020.ACL-MAIN.703>
- [11] Junnan Li, Dongxu Li, Caiming Xiong, and Steven C. H. Hoi. 2022. BLIP: Bootstrapping Language-Image Pre-training for Unified Vision-Language Understanding and Generation. In International Conference on Machine Learning, ICML 2022, 17-23 July 2022, Baltimore, Maryland, USA (Proceedings of Machine Learning Research, Vol. 162), Kamalika Chaudhuri, Stefanie Jegelka, Le Song, Csaba Szepesvári, Gang Niu, and Sivan Sabato (Eds.). PMLR, 12888–12900. <https://proceedings.mlr.press/v162/li22n.html>
- [12] Tsung-Yi Lin, Michael Maire, Serge Belongie, James Hays, Pietro Perona, Deva Ramanan, Piotr Dollár, and C Lawrence Zitnick. 2014. Microsoft coco: Common objects in context. In Computer Vision—ECCV 2014: 13th European Conference, Zurich, Switzerland, September 6–12, 2014, Proceedings, Part V 13. Springer, 740–755.
- [13] Shweta Mahajan, Tanzila Rahman, Kwang Moo Yi, and Leonid Sigal. 2023. Prompting Hard or Hardly Prompting: Prompt Inversion for Text-to-Image Diffusion Models. CoRR abs/2312.12416 (2023). <https://doi.org/10.48550/ARXIV.2312.12416> arXiv:2312.12416
- [14] Ron Mokady, Amir Hertz, and Amit H Bermano. 2021. Clipcap: Clip prefix for image captioning. arXiv preprint arXiv:2111.09734 (2021).
- [15] Alexander Quinn Nichol, Prafulla Dhariwal, Aditya Ramesh, Pranav Shyam, Pamela Mishkin, Bob McGrew, Ilya Sutskever, and Mark Chen. 2022. GLIDE: Towards Photorealistic Image Generation and Editing with Text-Guided Diffusion Models. In International Conference on Machine Learning, ICML 2022, 17-23 July 2022, Baltimore, Maryland, USA (Proceedings of Machine Learning Research, Vol. 162), Kamalika Chaudhuri, Stefanie Jegelka, Le Song, Csaba Szepesvári, Gang Niu, and Sivan Sabato (Eds.). PMLR, 16784–16804. <https://proceedings.mlr.press/v162/nichol22a.html>
- [16] Bryan A Plummer, Liwei Wang, Chris M Cervantes, Juan C Caicedo, Julia Hockenmaier, and Svetlana Lazebnik. 2015. Flickr30k entities: Collecting region-to-phrase correspondences for richer image-to-sentence models. In Proceedings of the IEEE international conference on computer vision. 2641–2649.
- [17] Alec Radford, Jong Wook Kim, Chris Hallacy, Aditya Ramesh, Gabriel Goh, Sandhini Agarwal, Girish Sastry, Amanda Askell, Pamela Mishkin, Jack Clark, Gretchen Krueger, and Ilya Sutskever. 2021. Learning Transferable Visual Models From Natural Language Supervision. In Proceedings of the 38th International Conference on Machine Learning, ICML 2021, 18-24 July 2021, Virtual Event (Proceedings of Machine Learning Research, Vol. 139), Marina Meila and Tong Zhang (Eds.). PMLR, 8748–8763. <http://proceedings.mlr.press/v139/radford21a.html>
- [18] Aditya Ramesh, Prafulla Dhariwal, Alex Nichol, Casey Chu, and Mark Chen. 2022. Hierarchical text-conditional image generation with clip latents. arXiv preprint arXiv:2204.06125 1, 2 (2022), 3.
- [19] Aditya Ramesh, Mikhail Pavlov, Gabriel Goh, Scott Gray, Chelsea Voss, Alec Radford, Mark Chen, and Ilya Sutskever. 2021. Zero-shot text-to-image generation. In International Conference on Machine Learning. PMLR, 8821–8831.
- [20] Robin Rombach, Andreas Blattmann, Dominik Lorenz, Patrick Esser, and Björn Ommer. 2022. High-resolution image synthesis with latent diffusion models. In Proceedings of the IEEE/CVF conference on computer vision and pattern recognition. 10684–10695.
- [21] Christoph Schuhmann, Richard Vencu, Romain Beaumont, Robert Kaczmarczyk, Clayton Mullis, Aarush Katta, Theo Coombes, Jenia Jitsev, and Aran Komatsuzaki. 2021. Laion-400m: Open dataset of clip-filtered 400 million image-text pairs. arXiv preprint arXiv:2111.02114 (2021).
- [22] Zeyang Sha, Zheng Li, Ning Yu, and Yang Zhang. 2023. Deepfake: Detection and attribution of fake images generated by text-to-image generation models. In Proceedings of the 2023 ACM SIGSAC Conference on Computer and Communications Security. 3418–3432.
- [23] Xinyue Shen, Yiting Qu, Michael Backes, and Yang Zhang. 2023. Prompt Stealing Attacks Against Text-to-Image Generation Models. CoRR abs/2302.09923 (2023). <https://doi.org/10.48550/ARXIV.2302.09923> arXiv:2302.09923
- [24] Zhimin Sun, Shen Chen, Taiping Yao, Bangjie Yin, Ran Yi, Shouhong Ding, and Lizhuang Ma. 2023. Contrastive Pseudo Learning for Open-World DeepFake Attribution. In Proceedings of the IEEE/CVF International Conference on Computer Vision. 20882–20892.
- [25] Andrey Voynov, Qinghao Chu, Daniel Cohen-Or, and Kfir Aberman. 2023. P+: Extended Textual Conditioning in Text-to-Image Generation. CoRR abs/2303.09522 (2023). <https://doi.org/10.48550/ARXIV.2303.09522> arXiv:2303.09522
- [26] Zhou Wang, A.C. Bovik, H.R. Sheikh, and E.P. Simoncelli. 2004. Image quality assessment: from error visibility to structural similarity. IEEE Transactions on Image Processing 13, 4 (2004), 600–612. <https://doi.org/10.1109/TIP.2003.819861>
- [27] Yuxin Wen, Neel Jain, John Kirchenbauer, Micah Goldblum, Jonas Geiping, and Tom Goldstein. 2023. Hard Prompts Made Easy: Gradient-Based Discrete Optimization for Prompt Tuning and Discovery. CoRR abs/2302.03668 (2023). <https://doi.org/10.48550/ARXIV.2302.03668> arXiv:2302.03668
- [28] Yuxin Wen, Neel Jain, John Kirchenbauer, Micah Goldblum, Jonas Geiping, and Tom Goldstein. 2023. Hard prompts made easy: Gradient-based discrete optimization for prompt tuning and discovery. arXiv preprint arXiv:2302.03668 (2023).
- [29] Tianyun Yang, Ziyao Huang, Juan Cao, Lei Li, and Xirong Li. 2022. Deepfake network architecture attribution. In Proceedings of the AAAI Conference on Artificial Intelligence, Vol. 36. 4662–4670.
- [30] Tianyun Yang, Danding Wang, Fan Tang, Xinying Zhao, Juan Cao, and Sheng Tang. 2023. Progressive Open Space Expansion for Open-Set Model Attribution. In Proceedings of the IEEE/CVF Conference on Computer Vision and Pattern Recognition. 15856–15865.

- [31] Ning Yu, Larry S Davis, and Mario Fritz. 2019. Attributing fake images to gans: Learning and analyzing gan fingerprints. In Proceedings of the IEEE/CVF international conference on computer vision. 7556–7566.

Received 28 January 2024; revised 12 March 2009; accepted 5 June 2009